Journal of Engineering Science and Technology
Vol. 10, No. 8 (2015) 994 - 1008
© School of Engineering, Taylor's University

EFFECT OF PROCESS PARAMETER VARIATION ON f_t IN CONVENTIONAL AND JUNCTIONLESS GATE-ALL-AROUND DEVICES

B. LAKSHMI[1,]*, R. SRINIVASAN[2]

[1]School of Electronics Engineering, VIT University, Chennai, India
[2]Department of Information Technology, SSN College of Engineering, Chennai, India
*Corresponding Author: laxmi.balu@yahoo.com

Abstract

In this paper we have studied the effect of process variations on unity gain cut-off frequency (f_t) in conventional and junctionless gate-all-around (GAA) transistors using TCAD simulations. Three different geometrical parameters, channel doping, source/drain doping (for conventional GAA), wire doping (for junctionless GAA) and gate electrode work function are studied for their sensitivity on f_t. For conventional GAA, f_t is more sensitive to gate length and source/drain doping and less sensitive to gate oxide thickness, ovality and channel doping and least sensitive to gate work function variations. For junctionless GAA, f_t is more sensitive to gate length and gate work function variations and less sensitive to gate oxide thickness, ovality, wire doping. The non-quasi static (NQS) delay is extracted for the most sensitive parameters. The trend of NQS delay is just the reverse trend of f_t.

Keywords: Gate-All-Around device, Junctionless GAA device, Non-Quasi Static delay, Unity gain cut-off frequency, TCAD.

1. Introduction

As downscaling of MOSFETs approaches the end of the ITRS, the silicon nanowire (SiNW) transistor with multi-gate or gate-all-around (GAA) architecture is attractive as one of the promising candidates for future CMOS technology. However as the device size is continuously scaled down, the formation of extremely abrupt junctions between source/drain and channel regions is still very challenging, even for the NW FETs when operating in the inversion-mode regime. But still, an ultrathin and narrow body (nanowire) MOSFET, when combined with the GAA structure, is deemed to be a major

Nomenclatures

C_{gg}	Gate Capacitance, fF
f_t	Unity gain cutoff frequency, GHz
g_m	Trans-conductance, mS
I_{off}	Off-state leakage current, A/μm
I_{on}	On-state drive current, μA/μm
L_g	Gate length, nm
N_{ch}	Channel doping, /cm^3
N_{SD}	Source/Drain doping, /cm^3
N_W	Wire Doping, /cm^3
T_{OX}	Gate oxide thickness, nm
V_{dd}	Supply voltage, V
V_{gs}	Gate Source Voltage, V
V_t	Threshold voltage, V

Abbreviations

CMOS	Complementary Metal Oxide Semiconductor
GAA	Gate All Around
ITRS	International Technology Roadmap for Semiconductors
NQS	Non-quasi static
SDE	Sentaurus Structure Editor
SDEVICE	Sentaurus Device
SiNW	Silicon Nanowire
TCAD	Technology Computer Aided Design
WF	Work Function

candidate for extreme CMOS scaling provided the process complexities such as fabrication of short wires and the gate definition under the body are solved [1]. To go below 10 nm, GAA transistors are seen as the best option.

The structure that theoretically offers the best possible control of the channel region by the gate, and hence the best possible Electrostatic Integrity is the surrounding-gate MOSFET. The reduction in channel width and thickness can further increase the effectiveness of the gate control, i.e., the gates can effectively control the electrostatic potential in the ultrathin channel, so that the channel suffers from lesser electrical interference between source and drain [2, 3]. Due to this, GAA device has enhanced drive current and sub threshold slope, as well as good immunity to short-channel effects.

There are some experimental results in the literature showing lithographically defined fully CMOS compatible silicon nanowire GAA device n- and p-MOS transistors with nanowire channel in different crystal orientations and characterized at various temperatures down to 5 K. These nanowire devices show high drive current, and excellent gate control with high I_{on}/I_{off} ratio. PMOS GAA device shows I_{on} enhancement along <010> orientation in comparison to conventional <110> direction [4]. The work function of the metal gate material used for GAA device is from 4.2 eV to 5.5 eV [5].

Literature is available for GAA, which can be particularly used for reducing the problems of conventional multi-gate FinFET, improving device performance

and scaling down capabilities [6, 7]. Surrounding-gate SOI MOSFETs with a gate length as small as 5 nm and a diameter of 3 nm have shown to be fully functional [8]. RF performance of GAA device has been investigated by [9]. Junctionless GAA devices have been explored recently [10, 11]. A systematic sensitivity analysis of conventional and junctionless GAA device RF performance is yet to be investigated. For RF applications unity gain cut-off frequency (f_t) is one of the important metric and it is the frequency at which $|Y_{21}/Y_{11}|$ ratio equals one. In terms of device parameters, f_t is given by g_m/C_{gg} where g_m is transconductance, C_{gg} is the combination of gate-source capacitance (C_{gs}), gate-drain capacitance (C_{gd}) and overlap capacitance (C_{ov}) [12].

In this paper, the effect of various process parameters on f_t is studied systematically. Three different geometrical parameters and three non-geometrical parameters (related to conventional GAA device) and two non-geometrical parameters (related to junctionless GAA device) are varied to capture their sensitivity on f_t. The non-quasi static (NQS) delay is extracted for the most sensitive parameters. The outline of this paper is as follows. Next section deals with the description and calibration of the devices. Section 3 explains about the parameter space for sensitivity study. Section 4 discusses the simulation results. Finally in Section 5 the conclusions are provided.

2. Device Description and Calibration

Sentaurus TCAD simulator from Synopsys [13] is used to perform all the simulations. All the simulations are carried out at 3D level. The device structures are generated using Sentaurus Structure Editor (SDE). Figure 1(a) shows the 3-D structure of the GAA device. The front view is shown in Fig. 1(b). The cross sectional views along the channel are given in Figs. 1(c) and (d), for conventional and junctionless GAA devices respectively. From Fig. 1(c) it can be seen that the channel is of p type doping and it has a doping concentration of $1\times10^{16}/cm^3$ whereas source/drain are n^+ doping and the doping concentration ranges to $1\times10^{20}/cm^3$. For Fig. 1(d), there is a uniform doping (n^+) of $6\times10^{19}/cm^3$ throughout the entire device.

Device simulator (SDEVICE) includes the appropriate models for band to band tunnelling, quantization of inversion layer charge, doping dependency of mobility, effect of high and normal electric fields on mobility, and velocity saturation. Standard AC simulations are done in SDEVICE and f_t is extracted from these results. As already stated, f_t is the frequency at which $|Y_{21}/Y_{11}|$ equals one, and it strongly depends on the gate bias. At various gate biases f_t is calculated and the maximum of them is taken as f_t. The current values of the two devices are calibrated against the ITRS [14]. The device dimensions are given in Table 1. From Table 1 it can be seen that the two devices differ with respect to their doping concentrations and work functions. Conventional GAA device has two different doping concentrations for channel ($1\times10^{16}/cm^3$) and source/drain ($1\times10^{20}/cm^3$) whereas junctionless GAA device has a uniform heavily doped concentration ($6\times10^{19}/cm^3$).

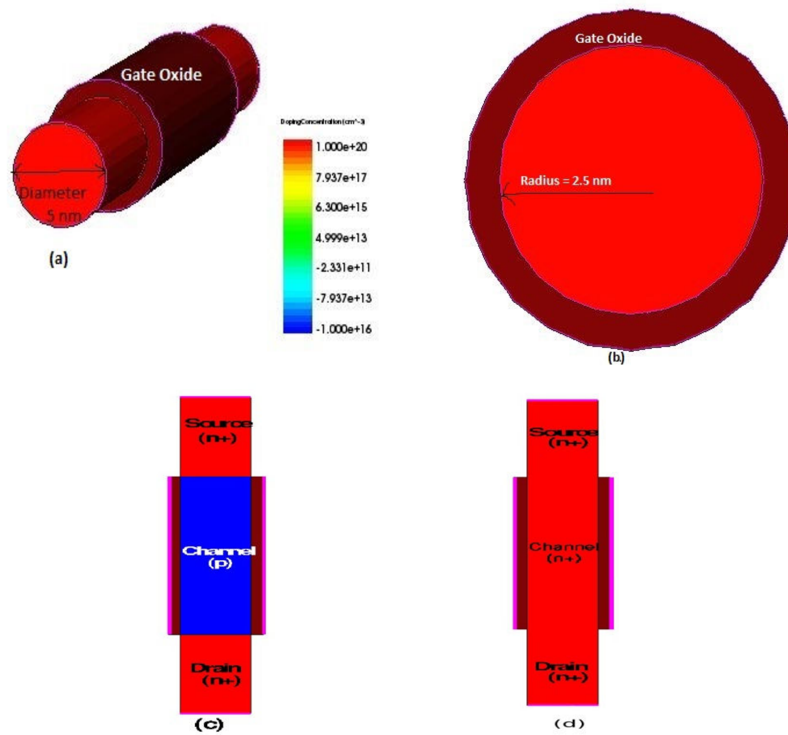

Fig. 1. (a) 3-D structure of GAA device (b) The front view of GAA device (c) Cross-sectional view along the channel of conventional GAA device (d) Cross-sectional view along the channel of junctionless GAA device.

Table 1. Dimensions of conventional and junctionless GAA.

Process Parameters	Conventional GAA device	Junctionless GAA device
Gate Length (L_g)	17 nm	
Diameter (D)	5 nm	
Gate oxide thickness (T_{ox})	0.77 nm	
Ovality	1 (ratio between major and minor axes)	
Channel doping (N_{ch})	1×10^{16}/cm^3	
Source/Drain doping (N_{SD})	1×10^{20}/cm^3	6×10^{19}/cm^3
Gate Work Function (WF)	4.27 eV	4.63 eV
Supply Voltage (V_{dd})	0.8 V	

Figure 2(a) shows the simulated I_d-V_g characteristics for conventional and junctionless GAA devices in log scale. Both the devices are matched to have same leakage current (I_{off}) of 100 nA/µm. Figure 2(b) shows the I_d-V_g characteristics in linear scale. It can be observed that the junctionless GAA devices have less drive current (1300 µA/µm for conventional GAA and 1056

μA/μm for junctionless GAA) compared to the conventional GAA devices for the same I_{off}. The mobility of junctionless devices is lower compared to inversion mode devices [15] and leads to higher drive current (I_{on}) in inversion mode devices. Since the carrier transport is in the bulk of the semiconductor, the current is reduced in the junctionless device. This in turn reduces the impact of imperfect semiconductor/insulator interfaces [16]. The extremely low leakage current is responsible for the susceptance of short channel effects in junctionless devices.

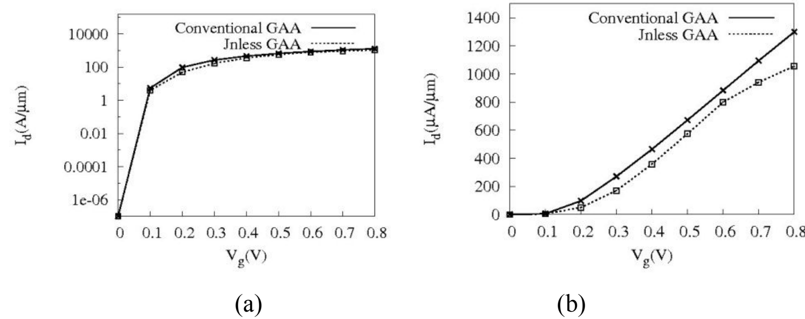

Fig. 2. (a) Simulated I_d-V_g characteristics of GAA devices of gate length 17 nm with I_{off} = 100 nA/μm (log scale) (b) Simulated I_d-V_g characteristics of GAA devices of gate length 17 nm (linear scale).

3. Parameter Space for Sensitivity Study

The process parameters considered here are gate length (L_g), gate oxide thickness (T_{ox}), ovality, channel doping (N_{ch}), source/drain doping (N_{SD}) and gate work function (WF). Ovality (non-circularity) is the degree of deviation from perfect circularity of the cross-section of the cylinder. These six parameters are varied over a range of values to capture their sensitivity on f_t for conventional and junctionless GAA devices. For junctionless devices, source/drain doping and channel doping are not considered separately and can be combined together called wire doping (N_W). Table 2 gives the range of values for the conventional and junctionless GAA devices.

Table 2. Range of values for the conventional and junctionless GAA devices.

<table>
<tr><th>Process Parameters</th><th>Conventional GAA device</th><th>Junctionless GAA device</th></tr>
<tr><td>Gate Length (L_g)</td><td colspan="2">10 nm - 30 nm</td></tr>
<tr><td>Gate oxide thickness (T_{ox})</td><td colspan="2">0.5 nm - 2 nm</td></tr>
<tr><td>Channel doping (N_{ch})</td><td>$1\times10^{15}/cm^3$ - $1\times10^{19}/cm^3$</td><td rowspan="2">$3\times10^{19}/cm^3$- $8\times10^{19}/cm^3$</td></tr>
<tr><td>Source/Drain doping (N_{SD})</td><td>$1\times10^{18}/cm^3$ - $2\times10^{20}/cm^3$</td></tr>
<tr><td>Gate Work Function (WF)</td><td>4.1 eV- 4.7 eV</td><td>4.6 eV - 5.1 eV</td></tr>
</table>

From Table 2 it can be seen that the doping concentration and work functions are varying for both the devices with their lower and upper bounds. For conventional GAA devices, channel doping concentration varies from 1×10^{15}/cm^3 to 1×10^{19}/cm^3 and source/drain doping concentration varies from 1×10^{18}/cm^3 to 2×10^{20}/cm^3. Since the doping concentration is uniform for junctionless GAA devices, it takes the value from 3×10^{19}/cm^3 to 8×10^{19}/cm^3.

4. Results and Discussion

4.1. Sensitivity Analysis with respect to f_t for conventional GAA device

As already stated, the six different process parameters are varied one at a time, and their sensitivity to f_t is analysed in this section.

Variation in gate length

Figure 3 shows the variation of f_t against gate length (L_g). Conventional GAA devices have a monotonic decrease with respect to L_g. This is the expected behaviour. This can be reasoned out with the g_m degradation for higher gate lengths.

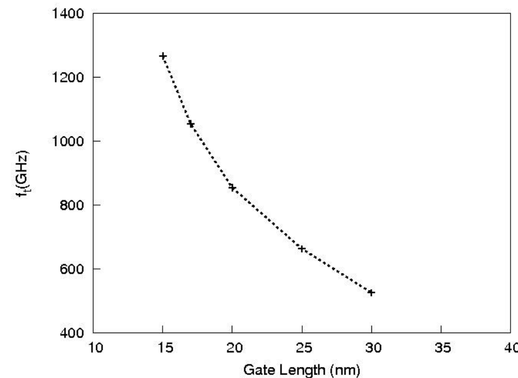

Fig. 3. Variation of f_t with respect to gate length in conventional GAA device.

Variation in gate oxide thickness

Figure 4 depicts the increase in f_t with respect to T_{ox}. Due to vertical gate electrical field, mobility degradation comes into picture with gate oxide scaling which ultimately decreases g_m although there is increase in C_{gg} [17]. Thus f_t decreases with gate oxide scaling.

Variation in ovality

Figure 5 depicts the variation of f_t with respect to ovality. It can be seen from Fig. 5 that there is a slight increase in f_t with respect to ovality. The variation in the ovality affects the channel width which in turn affects g_m. The increase in g_m increases f_t.

Variation in channel doping

Figure 6 shows the variation of f_t against N_{ch}. f_t is least sensitive at lower channel doping levels, similar to that of double gate FinFET, which is studied in [18]. At

higher doping levels, f_t is slightly decreasing due to g_m degradation. The same is seen in Fig. 6.

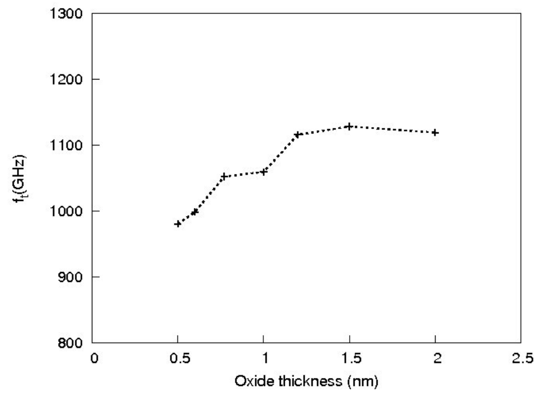

Fig. 4. Variation of f_t against gate oxide thickness in conventional GAA device.

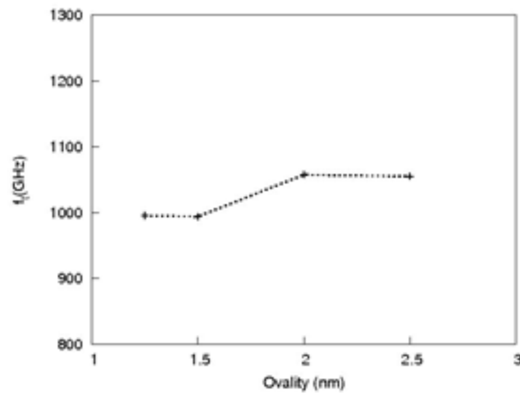

Fig. 5. Variation of f_t with respect to ovality in conventional GAA device.

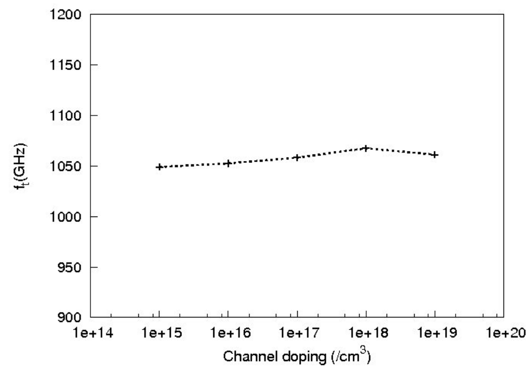

Fig. 6. f_t versus channel doping in conventional GAA device.

Variation in source/drain doping.

When N_{SD} increases, I_{on} and g_m increase due to the lowered parasitic series resistance and thereby f_t is expected to increase. Figure 7, which shows the variation of f_t with N_{SD}, reflects the same.

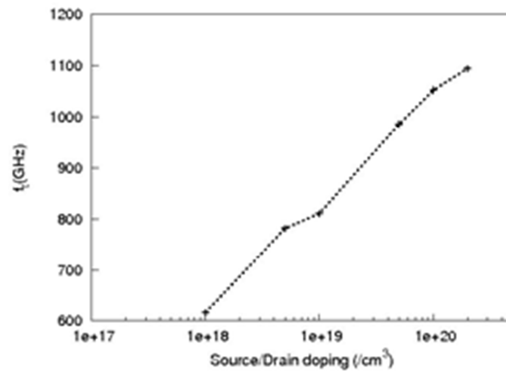

Fig. 7. f_t versus Source/drain doping in conventional GAA device.

Variation in gate work function

Screening effect is observed in the conventional GAA devices, similar to that of FinFET, which is explored by Lakshmi and Srinivasan [19]. Therefore, f_t is expected to be constant or least sensitive to gate electrode work function. The same can be observed in Fig. 8 which depicts the graph between f_t and work function.

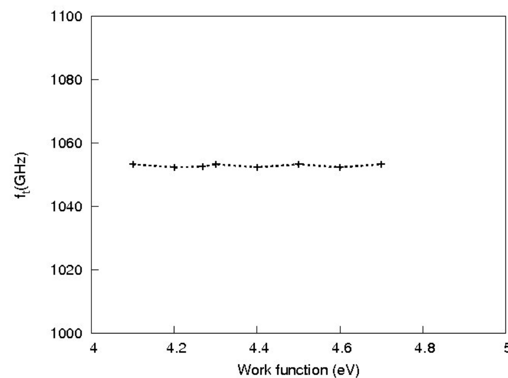

Fig. 8. Variation of f_t with gate electrode work function in conventional GAA device.

4.2. Sensitivity Analysis with respect to f_t for junctionless GAA device

The five parameters of junctionless GAA device are varied as shown in Table 2 and their sensitivity to f_t is analysed in this section.

Variation in gate length

Figure 9 shows the variation of f_t against gate length (L_g). Junctionless GAA devices have a monotonic decrease with respect to L_g. This can be reasoned out with the g_m degradation for higher gate lengths which is an expected result. From Fig. 9 it can be seen that the junctionless devices show lesser f_t (f_t= 620 GHz for L_g=20 nm) compared to the conventional devices (f_t= 850 GHz for L_g=20 nm) and this has been reported by Lakshmi and Srinivasan [20].

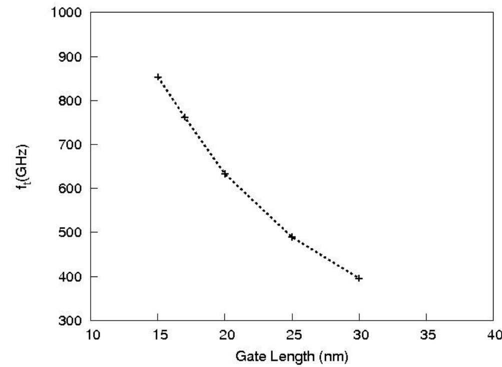

Fig. 9. Variation of f_t with respect to gate length in junctionless GAA device.

Variation in gate oxide thickness

Figure 10 shows the variation of f_t with gate oxide thickness (T_{ox}). The mobility degradation is less in the junctionless devices [21]. Therefore this device does not show any significant decrease for thin oxides.

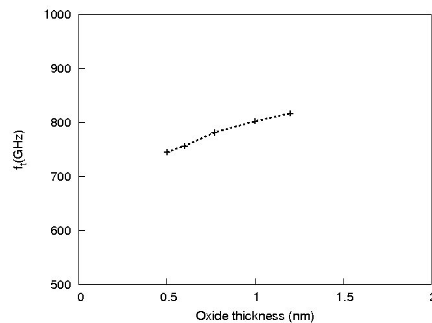

Fig. 10. Variation of f_t against gate oxide thickness in junctionless GAA device.

Variation in Ovality

Figure 11 depicts the variation of f_t with respect to ovality. Similar to the conventional GAA device, the variation in the ovality affects the channel width which in turn affects g_m thereby increases f_t slightly.

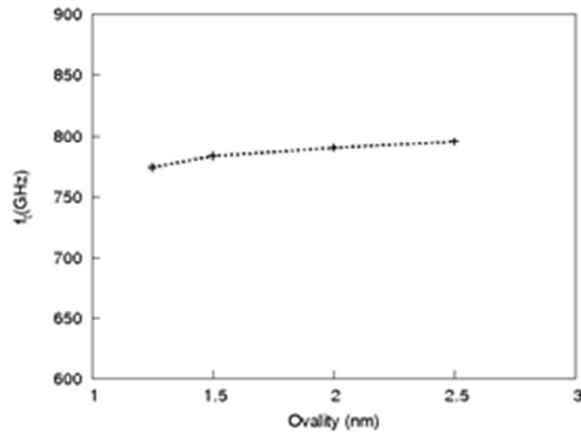

Fig. 11. Variation of f_t against ovality in junctionless GAA device.

Variation in Wire Doping

Figure 12 shows the variation of f_t against wire doping. For the junctionless devices, we can make the sensitivity study only for a limited range ($3x10^{19}/cm^3$ - $8x10^{19}/cm^3$). Beyond this range, f_t occurs at the extreme gate voltages, i.e., either at very low gate voltage or at V_{dd}. In this range, f_t is less sensitive to wire doping.

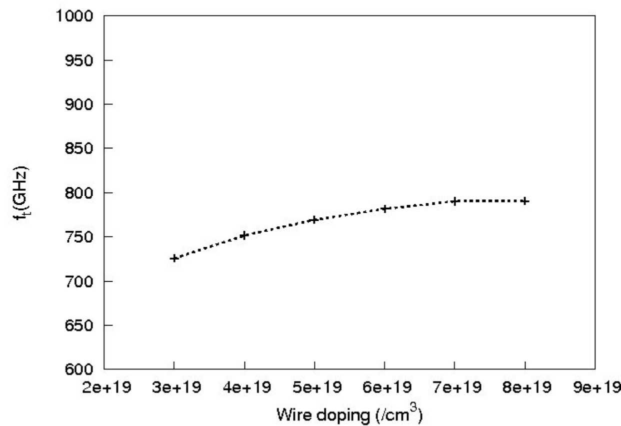

Fig. 12. f_t versus wire doping in junctionless GAA device.

Variation in gate work function

Figure 13 plots the variation of f_t with respect to gate work function. It can be observed that f_t starts to decrease after certain work function range. Junctionless devices have a strong dependency of f_t with respect to work function because there is no screening effect from the inversion region. Table 3 shows the classification of the various process parameters based on their sensitivity.

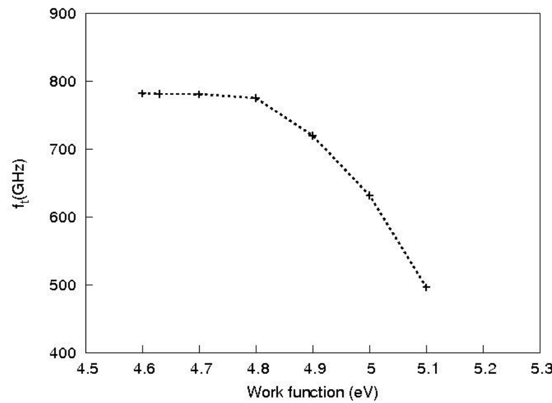

Fig. 13. Variation of f_t with gate electrode work function in junctionless GAA device.

Table 3. Classification of the Process Parameters based on their Sensitivity to f_t in Conventional and Junctionless GAA devices.

Conventional GAA device			Junctionless GAA device	
Gate Length	Oxide thickness	Gate Work function	Gate Length	Oxide thickness
Source/Drain Doping	Ovality		Gate Work function	Ovality
	Channel Doping			Wire doping

4.3. NQS delay for the sensitive parameters

For the sensitive parameters given in the Table. 3, NQS delay is extracted at a frequency of 200 GHz. To reason out the simulation result, the expression given by Allen et al [22] is used. For a particular NQS delay, the NQS frequency (f_{NQS}) is given by

$$f_{NQS} = \frac{\alpha \mu_{eff} (V_{GS} - V_t)}{2\pi L_g^2} \quad (1)$$

where α is the fitting parameter, μ_{eff} the mobility, V_{GS} the gate bias and V_t the threshold voltage of the transistor.

Conventional GAA device

The most sensitive parameters in conventional GAA device are found out to be L_g and N_{SD}. For these parameters alone, the NQS delay is extracted at a frequency of 200 GHz. Figure 14 shows the variation of NQS delay with respect to gate length. It can be seen that the delay increases with respect to L_g. Equation 1 predicts that

as L_g increases f_{NQS} decreases, i.e., for the given frequency NQS delay increases. Figure 15 shows the variation of NQS delay with respect to source/drain doping. The delay decreases for the variation in source/drain doping, which can be reasoned out similar to Fig. 7.

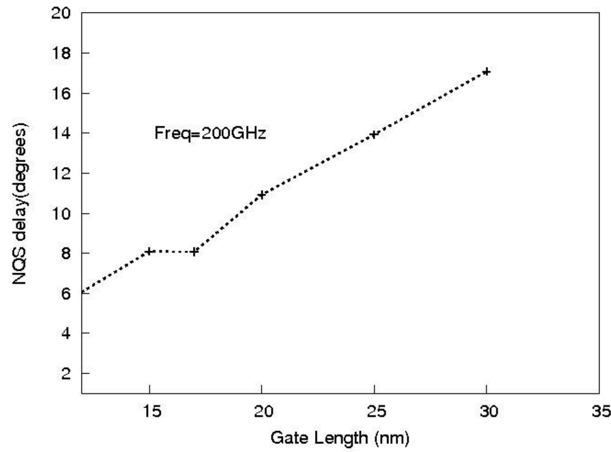

Fig. 14. NQS delay vs gate length in conventional GAA device.

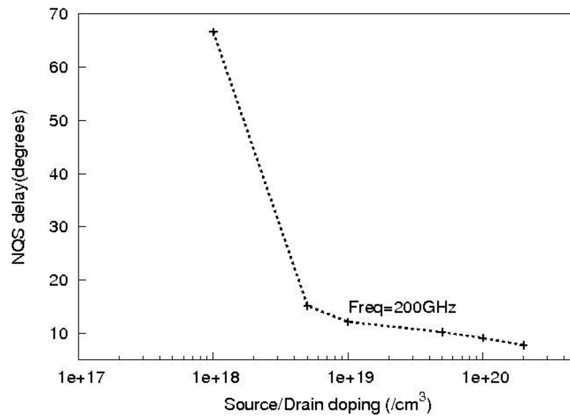

Fig. 15. NQS delay vs source/drain doping in conventional GAA device.

Junctionless GAA device

The most sensitive parameters in junctionless GAA device are found out to be L_g and WF. Figure 16 shows the variation of NQS delay with respect to gate length. As discussed previously, the delay increases monotonically with respect to gate length for junctionless GAA device also. Figure 17 shows the variation of NQS delay with respect to gate electrode work function. The increase in the

work function increases V_t, which ultimately increases the delay except for some initial values.

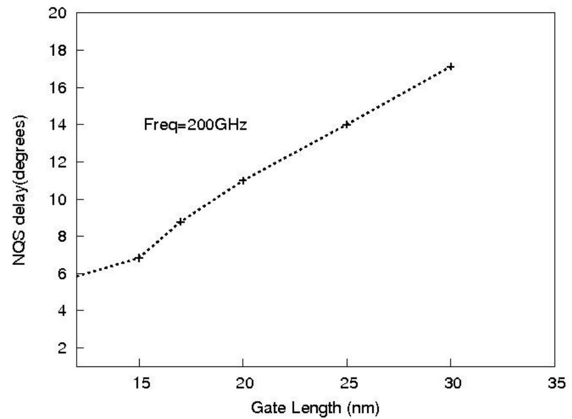

Fig. 16. NQS delay vs gate length in junctionless device.

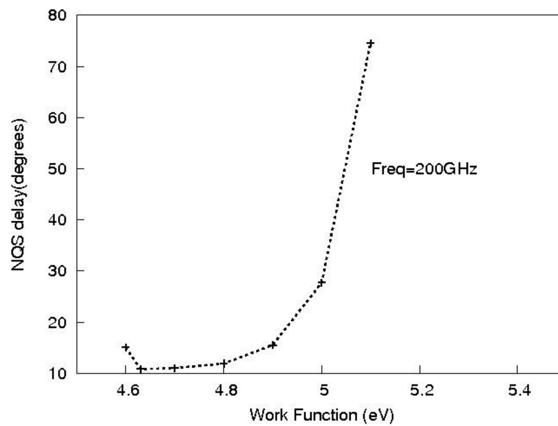

Fig. 17. NQS delay vs work function in junctionless GAA device.

5. Conclusion

In this paper, three different geometrical parameters and three non-geometrical parameters have been varied over a range and their effects on f_t have been studied for conventional and junctionless GAA. It was found that for conventional GAA, f_t is more sensitive to gate length and source/drain doping and less sensitive to gate oxide thickness, ovality and channel doping and least sensitive to gate work function variations. For junctionless GAA, f_t is more sensitive to gate length and gate work function variations and less sensitive to gate oxide thickness, ovality, wire doping. For the most sensitive parameters, NQS delay is extracted and the

trend followed by the NQS delay is just the reverse of f_t.

Acknowledgement

This work is supported by DRDO, Government of India.

References

1. Singh, N.; Agarwal, A.; Bera, L.K.; Liow, T.Y.; Yang, R.; Rustagi, S.C.; Tung, C.H.; Kumar, R.; Lo, G.Q.; Balasubramanian, N.; and Kwong, D.L. (2006). High performance fully depleted silicon nanowire (diameter ≤ 5 nm) gate-all-around CMOS devices. *IEEE Transactions on Electron Device Letters*, 27(5), 383-386.
2. Im, M.; Han, J.W.; Lee, H.; Yu, L.E; Kim, S.; Kim, C.H.; Jeon, S.C.; Kim, K.H.; Lee, G.S.; Oh, J.S.; Park, Y.C.; Lee, H.M.; and Choi, Y.K. (2008). Multiple-gate CMOS thin-film transistor with polysilicon nanowire. *IEEE Electron Device Letters,* 29(1), 102-105.
3. Clement, J.W.; Suk, S.D.; Li, M.; Yeoh, Y.Y.; Yeo, K.H.; Ha, J.K.; Lim, H.; Park, H.W.; Kim, D.W.; Chung, T.Y.; Oh, K.S.; and Lee, W.S. (2009). Characteristics of sub-5 nm trigate nanowire MOSFETs with single and poly Si channels in SOI structure. *Proceedings of VLSI Technology*, 142–143.
4. Singh, N.; Lim, F.Y; Fang, W.W.; Rustagi, S.C.; Bera, L.K.; Agarwal, A.; Tung, C.H.; Hoe, K.M.; Omampuliyur, S.R.; Tripathi, D; Adeyeye, A.O.; Lo, G.Q.; Balasubramanian, N.; and Kwong, D.L. (2006). Ultra-narrow silicon nanowire gate-all-around CMOS device: Impact of diameter, channel-orientation and low temperature on device performance. *Proceedings of IEDM*, 1-4.
5. Xiao, D.; Wang, X.; Yu, Y.; Chen, J.; Zhang, M.; Xue, Z.; and Luo, J. (2009). TCAD study on gate-all-around cylindrical (GAAC) transistor for CMOS scaling to the end of the roadmap. *Journal of Microelectronics*, 40(12), 1766-1771.
6. Lee, S.H; Yu, Y.S.; Hwang, S.W.; and Ahn, D. (2009). SPICE-compatible new silicon nanowire field-effect transistors (SNWFETs) model. *IEEE Transactions on Nanotechnology*, 8(5), 643-649.
7. Lai, W.T; Wu, C.W.; Lin, C.C.; and Li, P.W. (2011). Analysis of carrier transport in trigate Si nanowire MOSFETs. *IEEE Transactions on Electron Devices*, 58(5), 1336-1343.
8. Lee, H.; Yu, L.E.; Ryu, S.W.; Han, J.W.; Jeon, K.; Jang, D.Y.; Kim, K.H.; Lee, J.; Kim, J.H.; Jeon, S.C.; Lee, G.S.; Oh, J.S.; Park, Y.C.; Bae, W.H.; Lee, H.M.; Yang, J.M.; Yoo, J.J.; Kim, S.I.; and Choi, Y.K. (2006). Sub-5nm All-Around Gate FinFET for ultimate scaling. *Proceedings of VLSI Technology*, 58-59.
9. Zhuge, J.; Wang, R; Huang, R.; Xing, Z.; and Wang, Y. (2008). Investigation of parasitic effects and design optimization in silicon nanowire MOSFETs for RF applications. *IEEE Transactions on Electron Devices*, 55(8), 2142-2147.
10. Ansari, L.; Feldman, B.; Fagas, G.; Colinge, J.P.; and Greer, J.C. (2010). Simulation of junctionless Si nanowire transistors with 3 nm gate length. *Applied Physics Letters*, 97(6), 062105

11. Su, C.J.; Tsai, T.I.; Liou, Y.L.; Lin, Z.M.; Lin, H.C.; and Chao, T.S. (2011). Gate-all-around junctionless transistors with heavily doped polysilicon nanowire channels. *IEEE Electron Device Letters*, 32(4), 521-523.
12. Y. Tsividis (2009). *Operation and Modeling of the MOS Transistor* (2nd Ed.). Oxford University Press.
13. Synopsys Sentaurus Device User Guide. (2012-13)
14. International Technology Roadmap for Semiconductors. (2012)
15. Lee, C.W.; Borne, A.; Ferain, I.; Afzalin, A.; Yan, R.; Akhavan, N.D.; Razavi, P.; and Colinge, J.P. (2010). High temperature performance of silicon junctionless MOSFETs. *IEEE Transactions on Electron Devices*, 57(3), 620-625.
16. Han, M.H.; Chang, C.Y.; Chen, H.B.; Wu, J.J.; Cheng, Y.C.; and Wu, Y.C. (2013). Performance comparison between bulk and SOI junctionless transistors. *IEEE Electron Device Letters*, 34(2), 169-171.
17. Suryagandh, S.S.; Garg, M.; Gupta, M.; and Woo, J.C.S. (2004). Analog performance of scaled bulk and SOI MOSFETs. *Proceedings of Solid- State and Integrated Circuits Technology*, 153-158.
18. Xiong, S.; and Bokor, J. (2003). Sensitivity of double-gate and FinFET devices to process variations. *IEEE Transactions on Electron Devices*, 50(11), 2255-2261.
19. Lakshmi, B.; and Srinivasan, R. (2011). 3D-TCAD simulation study of process variations on f_t in 30 nm gate length FinFET. *Proceedings of ICETECT*, 589-593.
20. Lakshmi, B.; and Srinivasan, R. (2012). Investigation of f_t and non-quasi-static delay in conventional and junctionless multi-gate transistors using TCAD simulations. *ARPN Journal of Engineering and Applied Sciences*, 7(7), 847-852.
21. Colinge, J.P.; Lee, C.W.; Ferain, I.; Akhavan, N.D.; Yan, R.; Razavi, P.; Yu, R.; Nazalov, N.; and Doria, R.T. (2010). Reduced electric field in junctionless transistors. *Applied Physics Letters*, 96(7), 073510.
22. Allen, F.-L. Ng; Ko, P.K.; and Chan, M. (2002). Determining the onset frequency of non-quasi-static effects of the MOSFET in AC simulation. *IEEE Electron Device Letters*, 23(1), 37-39.